Chemical Engineering Journal 480 (2024) 147873

Contents lists available at ScienceDirect

Chemical Engineering Journal

journal homepage: www.elsevier.com/locate/cej

Process design, kinetics, and techno-economic assessment of an integrated liquid phase furfural hydrogenation process

Nerea Viar, Ion Agirre, Inaki Gandarias *

Department of Chemical and Environmental Engineering. Bilbao School of Engineering, University of the Basque Country (UPV/EHU), Plaza Ingeniero Torres Quevedo 1, 48013 Bilbao, Spain

ARTICLE INFO

Keywords:
Kinetic study
Langmuir-Hinshelwood
Furfuryl alcohol
Copper catalyst
Process intensification
Biorefinery

ABSTRACT

The integrated liquid phase process for producing furfuryl alcohol involves three stages: i) liquid–liquid extraction for recovering furfural from the aqueous solution obtained after a conventional steam-stripping hydrolysis reactor, ii) the hydrogenation reaction, and iii) the final purification. The reaction kinetics employed in the modelling are obtained experimentally. 2-methyltetrahydrofuran is the selected green solvent, and it has a high partition coefficient and stability under hydrogenating conditions. A commercial CuZnAl catalyst is used for the first time in the liquid phase furfural hydrogenation reaction, recording very high furfuryl alcohol selectivity even at complete conversion. A dual-site Langmuir-Hinshelwood model is developed and validated. An original aspect of this model is the kinetic effect of the low water content (0–5 wt%) remaining in the solvent after extraction. Water reduces the reaction rate by competing for active sites with furfural and furfuryl alcohol, without promoting other side-reactions. The optimization of the process leads to very high yields of furfuryl alcohol (97%) and a net production of 2-methyltetrahydrofuran even after recirculation and solvent losses. The process shows preliminary economic viability, with a minimum selling price for furfuryl alcohol of around 1,300 $/t; a competitive value only 30% higher than the furfural price considered in the analysis. Moreover, in contrast to current industrial processes that use copper chromite catalysts, the one developed here has environmental benefits, as it avoids the prior need for energy-intensive furfural-water distillation, eliminates toxic catalyst waste, and co-generates a green solvent.

1. Introduction

Furfural (FUR) is currently the main platform molecule derived from lignocellulosic biomass, with a global demand approaching 600 kilotons in 2020 [1]. The main producers are China, the Dominican Republic, and South Africa, which account for 90 % of global production [2]. The raw materials used are agricultural wastes with a high pentose content, such as bagasse or corncobs. FUR is obtained from the hydrolysis of pentoses into xyloses and their subsequent dehydration. The industrial production of FUR has hardly changed from the process developed by Quaker Oats in 1921 [3]. The reaction is accelerated by homogeneous acid catalysis, generally using mineral acids such as H_2SO_4. FUR is unstable and resinifies under operating conditions, so it is removed from the reactor by steam stripping. After condensing, an aqueous FUR (ca. 5–7 wt%) is obtained, which is purified by means of a high energy consuming double distillation [4]. The substantial energy cost of the process, low yields of around 50 %, and the use of mineral acids have meant that production in the European Union and the United States has declined significantly in recent years because of the need to compete with countries with lower energy prices and less restrictive environmental legislation [5].

FUR has a major potential as a platform molecule because it can be transformed into numerous compounds. Its aldehyde group can be reduced to alcohols, decarbonylated, oxidated to carboxylic acids, or undergo aldol condensation, acetylation, and acylation reactions [6]. Alternatively, its furan ring can be hydrogenated, alkylated, oxidized, halogenated, or nitrated [7]. However, most of these processes are still under development and have not reached industrial scale production. At present, 60–70 % of total FUR production is used to manufacture furfuryl alcohol (FOL, see Scheme 1), which is used as a monomer to obtain resins [8]. The later present exceptional mechanical, thermal, and chemical properties, and find application in the foundry industry [9].

FOL is produced industrially in either a liquid or vapor phase, but both routes start from purified FUR (i.e., 99.5 wt%). In the liquid phase,

* Corresponding author.
E-mail address: inaki.gandarias@ehu.eus (I. Gandarias).

https://doi.org/10.1016/j.cej.2023.147873
Received 28 September 2023; Received in revised form 10 November 2023; Accepted 2 December 2023
Available online 8 December 2023

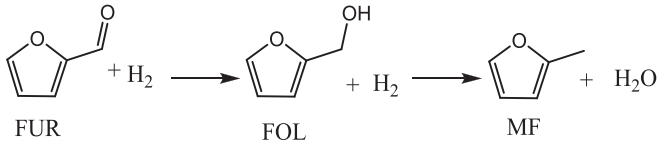

Scheme 1. Reaction pathway for the hydrogenation of furfural into furfuryl alcohol and its further hydrogenolysis reaction to yield 2-methylfuran.

the hydrogenation reaction is undertaken in a stirred tank reactor (STR), using copper-chromite as catalyst; the reaction is kept below 175 °C to minimize the formation of 2-methylfuran (MF, see Scheme 1) [10]. Moreover, CaO is added to the reaction medium to avoid resinification and side-reactions of FUR and FOL [11]. Although relatively high FOL yields (around 98 %) are obtained under these conditions, the process can be improved from an integration and environmental perspective. This study sets out to design and fine-tune a FOL production process to compete with current industrial ones, while reducing its environmental impact by minimizing the energy consumed in purification, reducing the use of chemicals, and substituting the hazardous catalyst.

An ideal solution would be the direct hydrogenation of the aqueous FUR obtained after the steam-stripping hydrolysis reaction. However, in the aqueous phase and at temperatures above 120 °C several side-reactions occur, such as the rearrangement of FUR to cyclopentanone [12,13], which sharply reduces process selectivity. Therefore, FUR needs to be extracted from water. Fig. 1 shows a schematic diagram of the proposed integrated process for producing FOL from the aqueous FUR obtained in a conventional steam-stripping hydrolysis reactor. First, FUR is extracted into an organic solvent. Next, this mixture is hydrogenated into FOL in a liquid phase reactor, and a final separation step yields the desired product and the solvent stream to be recirculated.

Solvents have a major impact on the activity and selectivity of FUR hydrogenation reactions [14], so it is important for the one selected to be stable under operating conditions and promote the desired reaction pathway. Hydrogen donors, such as ethanol [15] and 2-propanol [16], promote FUR conversion into MF; however, they are soluble in water and therefore unable to extract FUR. We have previously studied the extraction of FUR and its further transformation into MF, concluding that 2-methyltetrahydrofuran (MTHF) is the best candidate [17,18]. Besides its high FUR partition coefficient, its stability and promotion of the desired hydrogenation reaction, it can be obtained from biomass [19] and is considered a green solvent [20,21]. Hence, MTHF has been selected for the integrated process transformation of FUR into FOL.

Regarding the catalyst, copper-chromite should be avoided for environmental reasons. Copper is the preferred active metal for selectively obtaining FOL, as it promotes a perpendicular-ring mode adsorption configuration that hinders furan ring hydrogenation reactions [22]. Several chromite-free copper-based catalysts have been developed, such as Cu/SiO_2 [23], Cu-ZnO [24], Cu/Al_2O_3 [25], Cu/MgO [26] or Cu-Ni [27]. Although all these catalysts record high activity and selectivity at lab-scale, the use of a commercial catalyst has advantages in terms of proven viability at industrial scale, high structural stability for pelletizing, and low manufacturing costs. A commercial CuZnAl catalyst, HiFUEL® W220, has recorded higher activity and stability than commercial copper chromite under gas phase furfural hydrogenation [28]. Based on these results, we have selected the former for the liquid phase furfural hydrogenation kinetic study.

This study describes the design of the proposed integrated process involving the liquid–liquid extraction, reaction, and final purification steps. The design and fine-tuning of the reaction system has involved developing and validating a kinetic model using the aforementioned commercial chromite free CuZnAl catalyst. This kinetic model includes, for the first time, the effect of residual water present on the extract after the liquid–liquid extraction step. Several options are studied and compared in terms of energy demand and integration in the design of the purification train and recirculation. This study deals with the environmental issues surrounding current FOL industrial processes and develops a technically viable alternative for minimizing the energy consumption of the purification steps using a green solvent, and reduces toxic solid waste thanks to an ecofriendly catalyst. Finally, the economic analysis assesses the process's competitiveness and the main factors affecting the FOL minimum selling price (MSP).

2. Material & methods

2.1. Reaction kinetics

The FUR liquid-phase reaction was conducted over a commercial copper-based catalyst (HiFUEL® W220) purchased from Alfa Aesar. This catalyst was developed by Johnson Matthey and is used in Water-Gas Shift Reactions (WGSRs). The composition of the as-received catalyst pellets was 52 wt% CuO, 30 wt% ZnO, 17 wt% Al_2O_3, and 1 wt% activated carbon. Prior to the activity test, the catalyst was ground, sieved, and pretreated under a reductive hydrogen atmosphere. This step involved a tubular furnace, initially heated to 150 °C at a rate of 5 °C/min, subsequently raised to 230 °C at a rate of 1 °C/min, and finally maintained at this temperature for 1 h. The activity tests were performed using 50 mL autoclave reactors (Hastelloy) equipped with a glass insert and a magnetic stirrer. The 10 mL reaction solution consisted of 10–15 wt% FUR (Sigma Aldrich, 99 %) in MTHF (Sigma Aldrich, 99 %). Ultrapure water (Milli-Q®) was added in some experiments to study its effect in a concentration range from 1 to 5 wt%. The furfural-to-catalyst

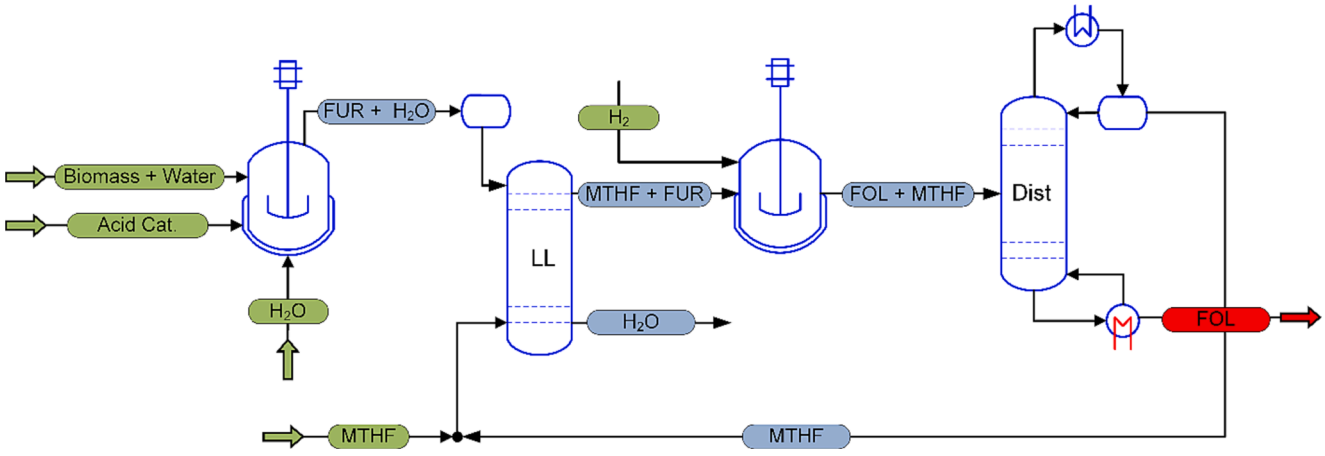

Fig. 1. Simplified flow diagram for the transformation of the aqueous furfural, obtained in a steam-stripping hydrolysis reactor, into furfuryl alcohol using 2-methyltetrahydrofuran as extracting and reaction solvent.

weight ratio was varied from 10 to 20, depending on the reaction temperature (105–135 °C). The reactor was purged three times to ensure there was no oxygen in the reaction environment and subsequently pressurized to achieve a hydrogen partial pressure of 30 bar at the reaction temperature. This pressure was kept constant throughout the reaction by connecting the reactors to a constant pressure hydrogen line. Once the set reaction time had elapsed, stirring was halted, and the reactor was cooled to room temperature. The reaction products were analyzed by a gas chromatograph (GC 6890 N Agilent) equipped with a flame ionization detector (FID), ~~with~~ using 1-pentanol as internal standard.

Reactant conversion and its selectivity towards products were determined by the following equations:

$$Conversion\,(\%) = \left(1 - \frac{n_{FUR}^{t}}{n_{FUR}^{t=0}}\right)\cdot 100 \quad (1)$$

$$Yield_i\,(\%) = \left(\frac{n_i^t}{n_{FUR}^{t=0}}\right)\cdot 100 \quad (2)$$

where n_i^t represents the moles of the product "i" at reaction time "t".

2.2. Process modelling, simulation, and techno-economic assessment

Process viability is assessed through a techno-economic analysis, encompassing its conceptual design, detailed mass and energy balance computations using established simulation tools such as Aspen Plus, cost estimation for both investment (CapEx) and operation (OpEx), and a sensitivity analysis to gauge the influence of any uncertain values.

2.2.1. Process modelling

The FOL production facility was designed according to existing industrial FUR production plants, which typically process several kilotons of FUR per year, with the largest capacity being 35 kilotons per year [7,29]. All the simulations here were based on an assumed annual availability of 20 kilotons of FUR producing approximately 19.8 kilotons of 99.0 wt% FOL per year.

Aspen Plus V12 software was used for process modeling. The UNIQUAC-HOC property method involving the UNIQUAC model for calculating liquid phase activity coefficients was coupled with the Hayden-O'Connell equation of state (EOS) [30,31] to determine the thermodynamic properties of the vapor phase. The UNIQUAC binary interaction parameters were acquired from two different sources. The interactions between water, MTHF, and FUR were based on regression analyses by Männistö et al. [30], using available experimental data. For those binary parameters lacking experimental data, the UNIFAC-LL group contribution method was used for the estimation [32].

The simulation of distillation towers was conducted according to the rigorous RadFrac model. The column stages were optimized using the minimum Total Annualized Costs (TAC) method [33], as described in Equation 3, which estimates the total OpEx, encompassing CapEx, amortization period, and utility costs.

$$TAC = \frac{Capital\ cost}{Payback\ period} + Utility\ costs \quad (3)$$

The optimal feed stage was identified by conducting a sensitivity analysis to minimize the reboiler duty. Reactors were simulated using the RCSTR kinetic model, integrating experimentally obtained kinetics.

A pervaporation (PV) unit was used to extract water from the organic phase. The membrane module was modeled with Aspen Custom Modeler V12 software, based on previously published governing equations and assumptions [34,35]. Prior experimental studies suggest that the permeation of organic compounds larger than C4 molecules is almost negligible when using HybSi® membranes under conditions similar to our study. Therefore, a previously validated Arrhenius-type permeance equation was specifically used for water [34–36].

2.2.2. Economic analysis

The economic analysis has considered CapEx and total OpEx, and the MSP of FOL [37] was used as a reference parameter for evaluating economic viability.

The MSP ensures that yearly earnings match the Equivalent Annual Operating Cost (EAOC) (Eq. 4). The EAOC, covering the annualized capital cost and OpEx, was computed using discounted cash flow analysis, considering a 10-year project duration, a targeted return rate of 20 %, and a 40 % tax rate [38]. The annualized CapEx (Eq. 5) was obtained by spreading the capital cost over the project's lifespan and added to the OpEx to provide the EAOC (Eq. 6).

$$MSP = \frac{Annualized\ capital\ cost + \ operating\ cost}{Plant\ FOL\ Production\ Capacity} \quad (4)$$

$$EAOC = Annualized\ capital\ cost + operating\ cost \quad (5)$$

$$Annualized\ capital\ cost = \frac{Capital\ cost\cdot i\cdot(1+i)^n}{(1+i)^n - 1} \quad (6)$$

where n = economic life of the plant (10 years).

i = internal rate of return (20 %).

The **CapEx analysis** followed standard methods [38], incorporating equipment costs provided by the Aspen Process Economic Analyzer (APEA-V12), using data from the first quarter of 2021. This module is incorporated into Aspen Plus and considers all equipment and installation costs, bulk plant installation such as the power distribution system and control system, and all indirect costs.

Membrane module costs, which were not available in APEA, were estimated based on the costs of Zeolite, a membranes found in the literature [39] and the cost of a membrane module calculated by the Dutch Association of Cost Engineers [40]. A conservative replacement period of three years was considered for the membranes [34]. However, given the mild operating temperatures in the current scenario, longer lifecycles might be feasible, potentially reducing the overall process cost. The CapEx covered equipment and installation expenses, indirect costs, contingency costs and fees, and auxiliary facilities. The purchased cost of steam ejectors was negligible [41], and carbon steel was assumed as the construction material [38].

The estimation of the **total OpEx** covered raw materials, utilities, catalyst, and additional expenses such as operating labor, maintenance, plant overheads, and administration costs [38]. Raw materials and utility costs were subject to an annual escalation factor of 3 %.

a) Raw materials

FUR, typically produced industrially from agricultural and forestry residues, involves using H_2SO_4 as a homogeneous catalyst for hydrolysis and dehydration. In most industrial processes, FUR is removed from the

Table 1
Principal costing parameters of the FOL production process.

Raw Materials	Price ($/t)	Consumption(CASE III without PV)	Consumption(CASE III with PV)
FUR [42]	1,000		
Aqueous FUR (7 wt %) [44]	800	273,785 t/year	273,785 t/year
MTHF [45,46]	1,800		
H_2 [45]	2,750	408.3 t/year	427.0 t/year
HiFUEL® (catalyst) [Johnson Matthey]	32,000	3,984 t/charge[a]	1.205 t/charge[a]
Utilities[b]			**Price**
Steam@0.45 MPa ($/kg)			0.0354
Electricity ($/kWh)			0.17114
Cooling Water[b] ($/GJ)			1.39
Secondary WWT ($/kg) [47]			0.184

[a]The catalyst is replaced every two years [37].
[b]Figures provided by a Spanish oil refining company (2023).

hydrolysis reactor by steam-stripping and further purified from water via double distillation [4]. The market price of FUR has fluctuated over recent years, ranging between 1,000–1,500 $/ton from 2012 to 2017 [42,43]. However, the FUR feed used here is directly obtained from the steam-stripping hydrolysis reactor (7 wt%), thus eliminating the need for the double distillation process. The cost saving achieved by directly using the FUR-water stream was estimated to be 196 $/ton [44]. Based on an assumed FUR price of 1,000 $/ton, the price of the FUR present in the 7 wt% aqueous phase would be 800 $/ton.

The price of the commercial CuZnAl catalyst was set at 32.0 $/kg, with a catalyst lifetime of two years [37]. Table 1 provides further details on catalyst costs and other raw material expenses.

b) Utilities

The utility prices used in the calculations were based on data for Q1 2023, provided by a **Spanish** oil refining company **(see** Table 1**)**. It was assumed that the cooling water was fed to the process units from a central facility comprising a cooling tower with fans, makeup water, chemical injection, and pumps. The calculations accounted for a windage loss of 0.3 % from mechanical draft towers, a maximum allowable salt concentration factor of 5, a pump power efficiency of 75 %, and a chemicals cost of 0.156$/1,000 kg of makeup water [38].

3. Results and discussion

This section is divided into four subsections. First, we proceed to design and fine-tune the LL extraction stage in which FUR is recovered from the aqueous phase obtained after a conventional hydrolysis-stripping stage. The results of this first section establish the objective for the subsequent kinetic study, as they determine FUR concentration and reveal the presence of water in the extract. The kinetic model developed here therefore includes the effect of residual water in the solvent. In the third subsection, we proceed to the design, modelling, integration, and fine-tuning of the process. A residual water removal step is designed accordingly, and then the kinetic model is used to optimize the reaction system as a function of water content. Subsequently, three possible cases are studied for the design of the purification train and solvent recirculation, and the one with the highest technical feasibility is selected. Finally, the last subsection presents an economic analysis of two scenarios, with or without water removal before the reaction, and the results are analyzed.

3.1. Design and fine-tuning of the liquid–liquid extraction section

As mentioned in the introduction, the production of FOL from FUR in aqueous phase yields undesirable by-products. Therefore, as the initial step, a liquid–liquid (LL) extraction process using MTHF was designed and fine-tuned to recover the aqueous FUR. Due to the high surface tension of the mixture (above 30 dyne/cm between 25 °C and 70 °C), a mixer-settler arrangement was chosen instead of a packed tower [38]. Prior to the design and fine-tuning, calculated equilibrium results for the water-MTHF-FUR system were compared to the experimentally reported ones [17] and validated.

The feed to the LL extraction unit has the typical characteristics obtained after a steam-stripping hydrolysis reaction in a conventional FUR facility. It consists of 7 wt% FUR in water, a temperature of 68 °C, and a pressure of 1 bar. Vapor-liquid–liquid equilibrium graphs (refer to Figures S1, S2, and S3 in the Supplementary Material) indicate that there are no advantages when operating the extraction units under vacuum or pressurized conditions. Under pressurized conditions, water is highly soluble in MTHF, thereby reducing process efficiency. In terms of temperature, the process is operated as close as possible to the azeotropic temperature to minimize the loss of MTHF during refining.

The target was to recover 99.5 % FUR in the organic phase, while maintaining a reasonable FUR concentration in the extract (approximately 15 wt%). Considering a stage efficiency of 80 %, a range of three to five separation stages was evaluated, as this type of arrangement is typically limited to a maximum of five stages [38]. Varying the amount of solvent fed into the process provided the required MTHF/FUR mass ratio for 99.5 % FUR extraction. The simulations showed that this ratio records values of 12.0, 7.6, and 6.1 when using three, four, and five stages, respectively (see Table **S1**). However, only with five stages was it possible to achieve 15 wt% FUR concentration in the extract stream. Under these conditions, the extract stream is at 71 °C and consists of 79.7 wt% MTHF, 15.0 wt% FUR, and 5.3 wt% water. Regarding the raffinate aqueous stream, it contains 5.7 wt% of MTHF solvent (1793.9 kg/h), which should be recovered and recycled because of its high cost (1,800 €/t [45,46]). A relatively simple distillation column was therefore used to recover 99 % of the MTHF from the raffinate. It should be noted that the purity of the recovered MTHF stream is 93 wt% due to the existing azeotrope with water. All the design specifications of this distillation column (C-103) are shown in Section 3.3.2.

3.2. Kinetics of liquid phase furfural hydrogenation

Determining the kinetic law and obtaining the kinetic and adsorption parameters are essential for modelling and fine-tuning the reaction system. Recent investigations have examined the kinetics of FUR hydrogenation in the liquid phase with copper-based catalysts. Some studies have proposed a first-order kinetic model [24,48–50], while others have developed a more complex mechanism based on the Langmuir-Hinshelwood-Hougen-Watson (LHHW) model [51,52].

A LHHW-based model has been proposed in this research and the reaction was studied at three different temperatures (105 °C, 120 °C, and 135 °C). The maximum temperature was established based on previous research [10,53], which indicates that the production of MF is enhanced above this temperature (see Scheme 1), decreasing the selectivity to our target product. A constant hydrogen partial pressure of 30 bar was maintained in all the experiments. This strategy has also been previously used [54,55]. The presence of water can affect the reaction rate. A previous study [22] has reported on the effect water has on the gas phase hydrogenation of FUR to FOL. It has been determined that water competes with other species for active sites without changing the adsorption equilibrium parameters of the other species. This effect was verified in the proposed liquid phase reaction system, by performing the kinetic study with and without water, which was varied from 0 to 5 wt%. The maximum water content studied corresponds to its concentration in the final extract stream of the LL extraction described in the previous section.

3.2.1. Mass transfer analysis

Prior to the kinetic study, different experiments were carried out varying the stirring speed to ensure that the reaction is governed by the kinetics and not by the external mass transfer resistance. The results are summarized in Figure S4. The initial reaction rate increased when the stirring speed was raised to 700 rpm. In this range, the reaction rate was limited by external diffusion. However, when increasing the speed above 700 rpm, the conversion remained constant, with negligible resistance from the external mass transfer. The stirring speed was therefore set at 700 rpm in the kinetic study. The catalyst was ground and sieved to a particle size smaller than 180 μm to avoid internal mass transfer resistance.

3.2.2. Reaction mechanism and rate law development

A kinetic model based on the LHHW mechanism was developed according to the following assumptions:

i. Molecular adsorption of FUR and FOL.
ii. Negligible adsorption of MF.
iii. Non-competitive dissociative adsorption of H_2 (dual site model).
iv. Surface reaction is the rate-determining step.
v. Both hydrogenation reactions are considered irreversible under the operating conditions studied.

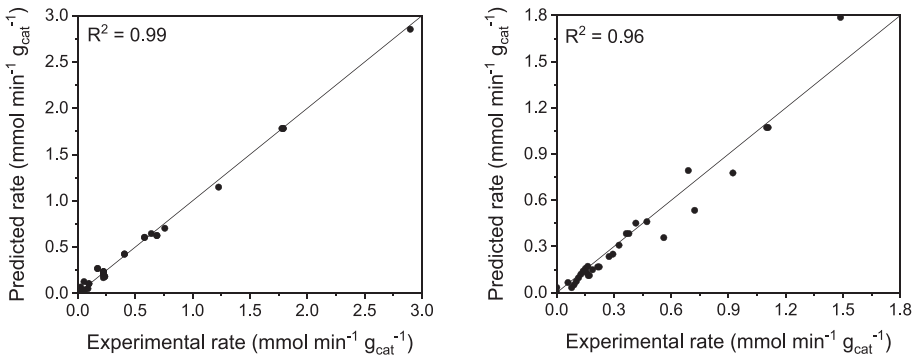

Fig. 2. Comparison of experimental and predicted rates at various temperatures without water (left) and with water in concentrations ranging 1–5 wt% (right).

This last assumption was thermodynamically confirmed by using Aspen Plus V12 software to determine the kinetic equilibrium constants for both reactions (see Table S2). Even at the highest temperature tested (135 °C), the calculated equilibrium constant for the FUR to FOL hydrogenation reaction is significant ($1.70{\cdot}10^2$), which under these operating conditions corresponds to an equilibrium conversion higher than 99.99 %. Regarding the dual site model, previous studies [49,56] on copper-based catalysts have reported that hydrogen is adsorbed on the metal active sites, while FUR is adsorbed on the acid sites. A commercial CuZnAl-based catalyst (W220) has been used, previously characterized by Jiménez-Gómez et al. [28], recording an acidity of 65 μmol NH_3/g_{cat}.

The assumption of negligible adsorption of MF is based on two factors. On the one hand, other authors have reported that the adsorption constant of MF is significantly lower than that of FUR and FOL [22]. On the other hand, given that this process is focused on FOL production, the reaction conditions (temperature and time) are fixed to minimize the production of MF, and hence, operate at very low MF concentrations.

Adsorption steps

$$FUR + S_1 \longleftrightarrow^{K_{FUR}} FUR{\cdot}S_1$$

$$H_2 + 2S_2 \longleftrightarrow^{K_{H_2}} 2H{\cdot}S_2$$

Surface reaction steps

Reaction 1: $FUR{\cdot}S_1 + 2H{\cdot}S_2 \xrightarrow{k'} FOL{\cdot}S_1 + 2{\cdot}S_2$

Reaction 2: $FOL{\cdot}S_1 + 2H{\cdot}S_2 \xrightarrow{k''} MF{\cdot}S_1 + H_2O + 2{\cdot}S_2$

Desorption steps

$$FOL{\cdot}S_1 \longleftrightarrow^{1/K_{FOL}} FOL + S$$

The proposed mechanism leads to the following rate expressions:

$$-r_{FUR} = k'{\cdot}\theta_{FUR}{\cdot}\theta_H^2$$

$$r_{FOL} = k'{\cdot}\theta_{FUR}{\cdot}\theta_H^2 - k''{\cdot}\theta_{FOL}{\cdot}\theta_H^2$$

$$r_{MF} = k''{\cdot}\theta_{FOL}{\cdot}\theta_H^2$$

where θ_{FUR}, θ_{FOL} and θ_{H2} are the fractional coverage of FUR, FOL, and hydrogen, respectively, defined as:

$$\theta_{FUR} = C_{FUR}{\cdot}K_{FUR}{\cdot}\theta_{v_1}$$

$$\theta_{FOL} = C_{FOL}{\cdot}K_{FOL}{\cdot}\theta_{v_1}$$

$$\theta_H = P_{H_2}^{1/2}{\cdot}K_{H_2}^{1/2}{\cdot}\theta_{v_2}$$

Performing the balance of active sites:

$$\theta_{v_1} = \frac{1}{1 + C_{FUR}{\cdot}K_{FUR} + C_{FOL}{\cdot}K_{FOL}}$$

$$\theta_{v_2} = \frac{1}{1 + P_{H_2}^{1/2}{\cdot}K_{H_2}^{1/2}}$$

Replacing the values on the rate expressions:

$$-r_{FUR} = \frac{k'{\cdot}C_{FUR}{\cdot}K_{FUR}{\cdot}P_{H_2}{\cdot}K_{H_2}}{(1 + C_{FUR}{\cdot}K_{FUR} + C_{FOL}{\cdot}K_{FOL}){\cdot}\left(1 + P_{H_2}^{1/2}{\cdot}K_{H_2}^{1/2}\right)^2}$$

The hydrogen partial pressure was kept constant during the kinetic experiments, so the P_{H_2} value in the numerator and the second term of the denominator are constant. Thus, the rate expressions become:

$$-r_{FUR} = \frac{k_1{\cdot}C_{FUR}{\cdot}K_{FUR}}{(1 + C_{FUR}{\cdot}K_{FUR} + C_{FOL}{\cdot}K_{FOL})}$$

Following the same procedure for the rate law of FOL and MF:

$$r_{FOL} = \frac{k_1{\cdot}C_{FUR}{\cdot}K_{FUR}}{(1 + C_{FUR}{\cdot}K_{FUR} + C_{FOL}{\cdot}K_{FOL})} - \frac{k_2{\cdot}C_{FOL}{\cdot}K_{FOL}}{(1 + C_{FUR}{\cdot}K_{FUR} + C_{FOL}{\cdot}K_{FOL})}$$

$$r_{MF} = \frac{k_2{\cdot}C_{FOL}{\cdot}K_{FOL}}{(1 + C_{FUR}{\cdot}K_{FUR} + C_{FOL}{\cdot}K_{FOL})}$$

As mentioned above, the kinetic study was also conducted when water was present in the reaction medium. The adsorption of water was considered on the same type of sites as that of FUR and FOL. It was assumed that water only partially covers the active sites, without affecting other parameters. An additional term was introduced into the kinetic model's denominator to account for the effect of water coverage.

$$-r_{FUR} = \frac{k_1{\cdot}C_{FUR}{\cdot}K_{FUR}}{(1 + C_{FUR}{\cdot}K_{FUR} + C_{FOL}{\cdot}K_{FOL} + C_{H_2O}{\cdot}K_{H_2O})}$$

$$r_{FOL} = \frac{k_1{\cdot}C_{FUR}{\cdot}K_{FUR}}{(1 + C_{FUR}{\cdot}K_{FUR} + C_{FOL}{\cdot}K_{FOL} + C_{H_2O}{\cdot}K_{H_2O})} - \frac{k_2{\cdot}C_{FOL}{\cdot}K_{FOL}}{(1 + C_{FUR}{\cdot}K_{FUR} + C_{FOL}{\cdot}K_{FOL} + C_{H_2O}{\cdot}K_{H_2O})}$$

$$r_{MF} = \frac{k_2{\cdot}C_{FOL}{\cdot}K_{FOL}}{(1 + C_{FUR}{\cdot}K_{FUR} + C_{FOL}{\cdot}K_{FOL} + C_{H_2O}{\cdot}K_{H_2O})}$$

3.2.3. Kinetic model analysis

Parity plots were generated to analyze and compare the fit between the experimental data and the predicted model. The results are summarized in Fig. 2. The results for the model are plotted without water on the left, while on the right they include the term for water adsorption on the active sites. A suitable correlation was established in both cases, with R^2 values exceeding 0.96.

In the case of water-containing experiments, the fitting process involved adjusting only the water coverage factor while keeping all the other parameters unchanged. This provided a suitable fit with the

Table 2
Kinetic and thermodynamic parameters for different temperatures.

	Rate constant (mmol min^{-1} g_{cat}^{-1})		Adsorption constant		
Temp (°C)	k_1	k_2	K_{FUR}	K_{FOL}	K_{H_2O}
105	0.24	$2.10 \cdot 10^{-3}$	102.00	8.87	75.54
120	0.73	$7.24 \cdot 10^{-3}$	24.29	5.04	28.46
135	3.35	$2.05 \cdot 10^{-2}$	4.77	2.01	7.69

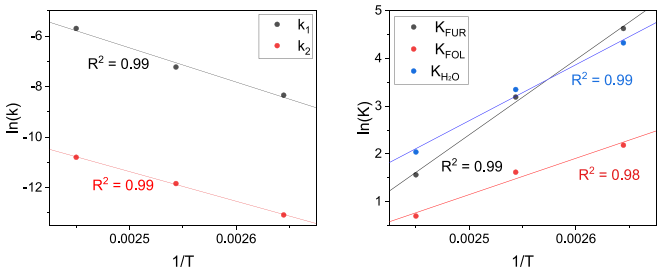

Fig. 3. Arrhenius plot for k_1 and k_2 (left) and Vańt Hoff plot for the adsorbed compounds (right).

experimental data, indicating that the following assumption was correct: when water is present in low concentrations (5 wt% or lower), it competes for active sites with FUR and FOL, thereby decreasing the reaction rate, but it does not promote the formation of other by-products. Indeed, the only by-product detected in any of the experiments was MF, and in very low yields. The reaction mixture remained transparent (without turbidity) and the carbon balance in all cases was in the 100 ± 3 % range. The very high selectivity with a water content equal to or lower than 5 wt%, even at complete conversion of the W220 commercial catalyst towards FOL, is better appreciated in the moles vs time plots in Figure S5. Water therefore reduces the reaction rate by competing for active sites, although it does not negatively impact catalyst selectivity.

The experimental data at each temperature were fitted to obtain the rate and adsorption constants, which are presented in Table 2. As expected, the rate constants increased with temperature, while the adsorption constants decreased. It is important to note that the rate constant of the FUR hydrogenation to FOL (k_1) is much higher, by around two orders of magnitude, than that of the subsequent hydrogenolysis of FOL to MF (k_2). This tendency has also been reported previously [52]. The results are interesting from a process perspective as it minimizes the production of MF and, hence, has a high selectivity to the desired product, FOL.

The FUR adsorption constant is much higher than that of FOL, which agrees with previous studies [26,57]. This fact also positively influences the selectivity of this compound under the reaction conditions studied. Moreover, as previously reported [22], water recorded a lower adsorption constant value compared to FUR at low temperatures, while at higher temperatures the constants tend to equalize.

The activation energy and pre-exponential factor of the hydrogenation of FUR to FOL (reaction 1) and hydrogenolysis of FOL to MF (reaction 2) were determined by fitting the data to the Arrhenius equation (see Fig. 3 and Table 3). The activation energy for the hydrogenation of FUR to FOL is comparable with other reported copper catalysts, as indicated in Table S3. The value is slightly higher than some of the reported ones, albeit within the same range, which renders the catalyst suitable for the process.

The activation energy for both reactions was comparable, which aligns with previous work [22,52]. However, there was a significant difference in the pre-exponential factor. The first reaction recorded a significantly larger factor, resulting in a higher reaction rate, as stated previously. The Vańt Hoff plot (Fig. 3) was used to calculate the thermodynamic parameters outlined in Table 3. The FUR adsorption heat is higher than that of FOL, which is in close agreement with previous research [22,52,57].

In short, the commercial chromite-free W220 catalyst has been used for the first time in the hydrogenation of FUR to FOL in liquid phase. The results are very promising because of the high selectivity obtained even at near complete conversions. One of the key objectives in a catalytic process is to ensure its activity and selectivity towards the target product, simplifying the subsequent product separation and purification by minimizing the generation of by-products. In this regard, the chromite-free commercial catalyst used had a high potential. The dual site LHHW model developed here fits the experimental data and can be used to accurately model the reaction section. Moreover, the kinetic study is pioneering by including for the first time the effect of residual water in the solvent, which reduces the reaction rate by competing for active sites with FUR and FOL, but does not promote the formation of other by-products.

3.3. Design, integration, and fine-tuning of the FOL production process

3.3.1. Effect of water removal before the reaction section

Based on the kinetic study described in Section 3.2, water plays an important role by competing for active sites with FUR and FOL. Its presence slows the reaction rate, which has an important effect when defining the reaction section. Water removal prior to the reaction system leads to a faster reaction rate, and therefore smaller reactors and/or lower catalyst consumption.

A pervaporation (PV) module was modeled for water removal considering two different approaches: i) an isothermal module, and ii) an adiabatic module. The feed to the pervaporation module is the outlet stream of the LL extraction section (extract) with a total mass flowrate of 15,176.8 kg/h at 73 °C and under 1 bar (79.7 wt% MTHF, 15.0 wt% FUR, 5.3 wt% water). The first estimations indicate that both types of modules can easily remove 90 % of water. For the isothermal case, 250 m^2 of membrane area would be necessary, with 1200 m^2 required for the adiabatic one. In both cases, the permeate pressure was kept constant at 56 mbar. One of the reasons for such a high membrane area is the huge temperature drop between the feed and retentate streams (from 73 °C to 16 °C). In the isothermal case, an additional energy (low pressure steam) of 0.47 MW is required to keep the temperature constant. However, this energy cost is much lower than the savings associated with 950 m^2 of membrane area (difference between the required membrane area in an adiabatic PV module and an isothermal PV module), which, in turn, should be replaced periodically (see Table S4).

The reaction section was studied based on these results and the kinetic study. Different CSTRs placed in series were considered to maximize the FOL yield. The first reactor works under adiabatic conditions,

Table 3
Kinetic and thermodynamic parameters for different temperatures.

Kinetic parameters			Adsorption thermodynamic parameters			
	Reaction 1	Reaction 2		FUR	FOL	H_2O
Activation energy (kJ mol^{-1})	$1.13 \cdot 10^2$	$9.76 \cdot 10^1$	ΔS_{ads} (kJ/mol K^{-1})	$-3.07 \cdot 10^{-1}$	$-1.48 \cdot 10^{-1}$	$-2.22 \cdot 10^{-1}$
Pre-exponential factor (mol min^{-1} g_{cat}^{-1})	$8.02 \cdot 10^{11}$	$6.47 \cdot 10^7$	ΔH_{ads} (kJ/mol)	$-1.31 \cdot 10^2$	$-6.33 \cdot 10^1$	$-9.75 \cdot 10^1$

Table 4
FUR conversions and FOL yields when varying the number of reactors and residence time (t_r). **In bold**, the selected values for each scenario.

Without water removal	**t_r (min)**																			
						5					**10**					**15**				
	Outlet of reactor	**1**	**2**	**3**	**4**	**5**	**1**	**2**	**3**	**4**	**5**	**1**	**2**	**3**	**4**	**5**	**1**	**2**	**3**	**4**	**5**
	X	46.5	70.7	83.7	90.8	94.8	64.0	86.6	94.9	98.1	**99.3**	71.6	91.6	97.5	99.2	99.8
	FOL yield	46.4	70.4	83.2	90.1	93.9	63.7	85.8	93.7	96.4	**97.1**	71.0	90.4	95.6	96.6	96.5
	MF yield	0.1	0.3	0.5	0.4	0.9	0.3	0.8	1.2	1.7	**2.2**	0.6	1.2	1.9	2.6	3.3
With 90 % water removal	**tr (min)**	**4**					**5**					**10**									
	Outlet of reactor	**1**	**2**	**3**	**4**	**5**	**1**	**2**	**3**	**4**	**5**	**1**	**2**	**3**	**4**	**5**					
	X	69.7	91.0	97.4	**99.2**	99.8	74.4	93.6	98.4	99.6	99.9	85.4	97.9	99.7	100.0	100.0					
	FOL yield	69.3	90.0	95.6	**96.8**	96.7	73.8	92.1	96.1	96.5	96.0	83.9	94.8	95.0	93.7	92.2					
	MF yield	0.4	1.0	1.8	**2.4**	3.1	0.6	1.5	2.3	3.1	3.9	1.5	3.1	4.7	6.3	7.8					

while the downstream ones work under isothermal conditions, as the amount of heat to be removed from them is minimal. The inlet temperature for the first reactor was set to operate at 135 °C, the temperature for recording the best experimental results. All the reactors were connected to a hydrogen supply by means of a valve, so only the required hydrogen is consumed, keeping the hydrogen partial pressure constant inside the reactors at 30 bar. It was assumed that the liquid phase occupies two thirds of the reactor volume. The industrial window of 0.1–10 tons of FOL per reactor cubic meter and per hour of catalyst activity was considered to estimate the catalyst amount to be placed in each reactor [58]. The simulations used 93 kg of catalyst/$m^3_{reactor}$ for an average reaction rate (50 % of conversion at 135 °C and 1.25 wt% of water content).

Table 4 shows the FUR conversion recorded, together with the FOL and MF yields when modifying the number of reactors and/or the residence time. Two scenarios were studied: i) direct use of the extract stream fed from the LL extraction unit with no water removal, (79.7 wt% MTHF, 15.0 wt% FUR, 5.3 wt% water) and ii) after removing 90 % of the water in the PV unit (83.7 wt% MTHF, 15.7 wt% FUR, 0.5 wt% water). As expected, shorter residence times are required, with lower water content to achieve equivalent FUR conversions. However, water removal also affects the FOL yield. The availability of more active sites produces more MF, slightly decreasing FOL yield at high residence times. This case considered the configuration in which at least 99 % of FUR conversion was recorded, and it also provided the highest FOL yield. Thus, the scenario without water removal requires five reactors with a residence time of 10 min in each one. The scenario in which 90 % of water was removed required only four reactors with four minutes of residence time to record similar yields. These results also influence the volume of the reactors, as well as the amount of catalyst in each one. For the scenario without water removal, the volume and catalyst loading of each reactor are 4.5 m^3 and 422 kg, respectively, while for the water removal scenario, these figures are 3.1 m^3 and 292 kg, respectively.

Water removal prior to the reaction section clearly has a positive effect from a technical point of view because fewer and smaller reactors are required, and therefore lower catalyst loadings. However, it needs to be ascertained whether the associated cost savings are higher than the costs associated with the installation of the aforementioned PV module. The following section studies different process integration options without water removal. The one recording the most promising results will be economically assessed in section 3.4, considering the possible incorporation of the PV module.

3.3.2. Process integration and optimization

Section 3.1 describes how 15 wt% of FUR in MTHF can be obtained from an aqueous 7 wt% of FUR through an LL extraction process,. A kinetic study considering different water concentrations (0–5 wt%) leads to the fine-tuning of the reaction system, with the possibility of using a water PV membrane module upstream of the reaction system. The next step in an integrated process involves FOL purification and the recovery of MTHF to be recycled in the process. At least one distillation column (C-101) is required accordingly. The design specifications were set to obtain 99 % FOL recovery with a purity of 99.0 wt%, varying the reflux ratio and the distillate-to-feed ratio. This distillation was simulated under vacuum conditions (0.2 bar) to avoid the formation of FOL-derived resinous by-products (above 175 °C) [10]. Under this slight vacuum, FOL can be recovered from the bottom at 123 °C, while the MTHF leaves the distillation column from the top at 33 °C, enabling the use of cooling water in the condenser. All the design specifications of this separation unit are summarized in Table 5 together with the main equipment data.

MF is also produced in the reaction section, and despite its low yield (<2.5 %) it leaves the distillation column C-101 together with MTHF and water. MF is not purged/consumed when this stream is recirculated in the LL extraction section, and therefore accumulates. Three different cases were considered to avoid this situation:

Table 5
Design specifications and calculated data for FOL purification.

	C-101	C-101(with a previous PV module)	C-103
Key compound bottom	FOL	FOL	–
Key compound distillate	–	–	MTHF
Key compound purity (wt%)	99	99	93
Pressure (bar)	0.2	0.2	0.2
Boiler Temperature (°C)	122	123	59
Condenser Temperature (°C)	31	33	31
Equilibrium stages (reboiler included)	5	5	7
Real stages (reboiler included)	8	8	10
Feed stage	3	3	4
Reflux ratio	0.02	0.05	2.0
Reboiler duty (kW)	910.3	676.3	396.7
Condenser duty (kW)	−1885.7	−1436.3	−733.5
Distillate-to-feed ratio (mole)	0.89	0.86	0.016
Column diameter (m)	2.1	1.8	1.4
Column height (m)	7.3	7.3	9.1
Heating Utility	LP-steam	LP-steam	LP-steam
Heating utility flow (kg/s)	0.4	0.3	0.18
Cooling Utility	Water	Water	Water
Cooling utility flow (kg/s)	90.3	68.8	35.1

- CASE I: Purge part of the C-101 distillate stream (see Fig. 4a).
- CASE II: Separate MF from MTHF by means of distillation in C-102 (see Fi. 4b).
- CASE III: Convert MF into MTHF in a downstream hydrogenating R-106 (see Fig. 4c).

In Case I, three different purge ratios were assayed, 1 %, 2.5 % and 5 %. These percentages meant the resulting MF wt% at the inlet of the reaction system was very high (22.6 %, 10.0 %, and 5.0 %, respectively). This option was rejected because high purge ratios were required to maintain low MF concentrations in the process, with the high cost of feeding fresh MTHF to replace solvent losses.

Case II considered the separation of MF from MTHF by means of a second distillation column (C-102). The design specifications were set for a 75 % MF mole recovery from the top of the column and a MTHF mole recovery of 99.5 wt% from the bottom. The reflux ratio and the distillate-to-feed ratio were therefore varied. In this case, distillation was simulated under atmospheric pressure, recording an MTHF stream (93 wt% MTHF and 6.2 wt% water) from the bottom at 70 °C and a MF stream from the top (36.7 wt% MF, 53.3 wt% MTHF, and 10.0 wt% water) at 61 °C. It was technically possible to record a higher MF recovery ratio, but the required energy rendered it unviable. The specified separation meant MF concentration at the reaction system inlet was stabilized at 0.1 wt%, but at the cost of significant MTHF loss. All the design specifications for this separation unit are summarized in Table **S5** together with the main equipment data.

The by-product MF In Case III was hydrogenated into MTHF in an additional reactor, R-106, placed downstream of the FOL purification C-101. The kinetic data published by Sivec et al. have been applied for the design of this reactor [51] due to the similarity of the reaction conditions. These scholars have experimentally tested various Cu, Ni, Pd, Pt, Re, Rh and Ru-based carbon supported catalysts in the hydrogenation, hydrodeoxygenation, and ring-opening of FUR using tetrahydrofuran as solvent, with the conversion of MF into MTHF being one of the steps in their reaction pathway. A Pd/C catalyst hydrogenated the furan ring of MF into MTHF even at 100 °C. Although this kinetic study was performed at various temperatures (100 °C, 150 °C, and 200 °C), the lowest temperature was chosen here for the hydrogenation of MF into MTHF due to the small amount of MF to be converted. The design results show that a single CSTR-type reactor (0.3 m^3) is required to convert 90 % of MF at 100 °C under 60 bar of H_2, 1 min of residence time and 2.5 kg of catalyst. The great advantage here involves cost savings related to MTHF. In the two previous cases, and to a greater or lesser extent, fresh MTHF needs to be fed into the process to offset any solvent losses. However, in this latter case, MTHF formation not only compensates for the losses but also provides a net production. This MTHF surplus was extracted from the process as a possible marketable product.

Comparing CASE II and CASE III, the latter seems to be the more promising one, not only due to its net solvent production, but also because of a lower energy requirement (see Table 6). Moreover, the capital costs related to a 0.3 m^3 CSTR are much lower than the costs of the aforementioned distillation column. The following section therefore presents the final techno-economic assessment of the two scenarios in CASE III: i, without a water PV membrane (Fig. 4c) and with one (Fig. 5).

3.4. Techno-economic assessment

Fig. 6 shows the EAOC calculated for both scenarios, with a PV membrane module (CASE III-a) and without one (CASE III-b). The capital cost (grey plain block) accounts for 11 % of the total EAOC, which is around 25 M$/year in both cases.

Section 3.3.1 concluded that water removal upstream of the reaction section was advantageous from a kinetic perspective, reducing the CSTRs required from five to four, and also shortening the residence time from 10 to 4 min. However, it needed to be ascertained whether these cost savings were higher than the costs associated with the installation of a PV module. Table 7 provides a more detailed view of the cost of the installed equipment divided by each section for CASE III-a and CASE III-b. The cost of the membrane module in CASE III-b cancels out the aforementioned savings in the reaction section. The sum of the costs associated with the reaction section and the PV membrane module in CASE III-b is slightly higher than the cost of the plant's reaction section in CASE III-a (with no membrane), and it is an expensive section (38–39 % of CapEx), just behind the cost associated with the LL extraction process (42–44 %).

The OpEx itemized in Table 7 reveal that raw materials account for 73 % (16.6 M$/year) in both scenarios. There is a slight increase in utility costs in CASE III-b due to the continuous energy supply (0.46 MW) required to maintain the PV membrane module at a constant temperature of 71 °C. The membrane replacement cost (0.5 %) and catalyst cost are practically negligible, although the catalyst cost in CASE III-b is three times lower than in CASE III-a (126.7 $/year vs 38.3 $/year). The energy requirements related to the FOL purification distillation column (C-101) are 30 % lower in CASE III-b than in CASE III-a (see Table 5). Hence, after calculating the costs of operating labor, maintenance, overheads (4.5 M$/year), the OpEx figure is around 22.7 M$/year.

One of the advantages of CASE III is the net production of MTHF. When no water was removed (CASE III-a), 173.4 t/year of 93.5 wt% MTHF are produced, while 226.8 t/year of 99.0 wt% MTHF are produced with a PV module (CASE III-b),. The latter yield could be sold directly on the market. Considering an MTHF price of 1,800 $/t [45,46], around 0.4 M$/year could be obtained as revenue. In the case of the 93.5 wt% MTHF stream, a study should be conducted to ascertain whether it is worth upgrading or it should be treated as waste. In this latter case, wastewater treatment costs of around 32,000 $/year should be added. Therefore, the MSP for FOL, calculated as defined in section 2.2, was 1,349 $/t in CASE III-a, and 1,326 $/t in ASE III-b. Given the minor difference between the MSP calculated for these two scenarios, it is not possible to state which of the two options is more appropriate. However, as the only difference between the processes is the presence of a PV module, and a conservative membrane replacement period was chosen (every three years), the option in which a PV module is incorporated could provide a more positive outcome. The FOL market price fluctuates with the FUR price, varying between 30 and 40 % higher than FUR [59]. These preliminary calculations show that the process developed here is technically and economically viable. A FUR market price of 1,000 $/T provided an MSP of 1,326 $/t. Moreover, it has important

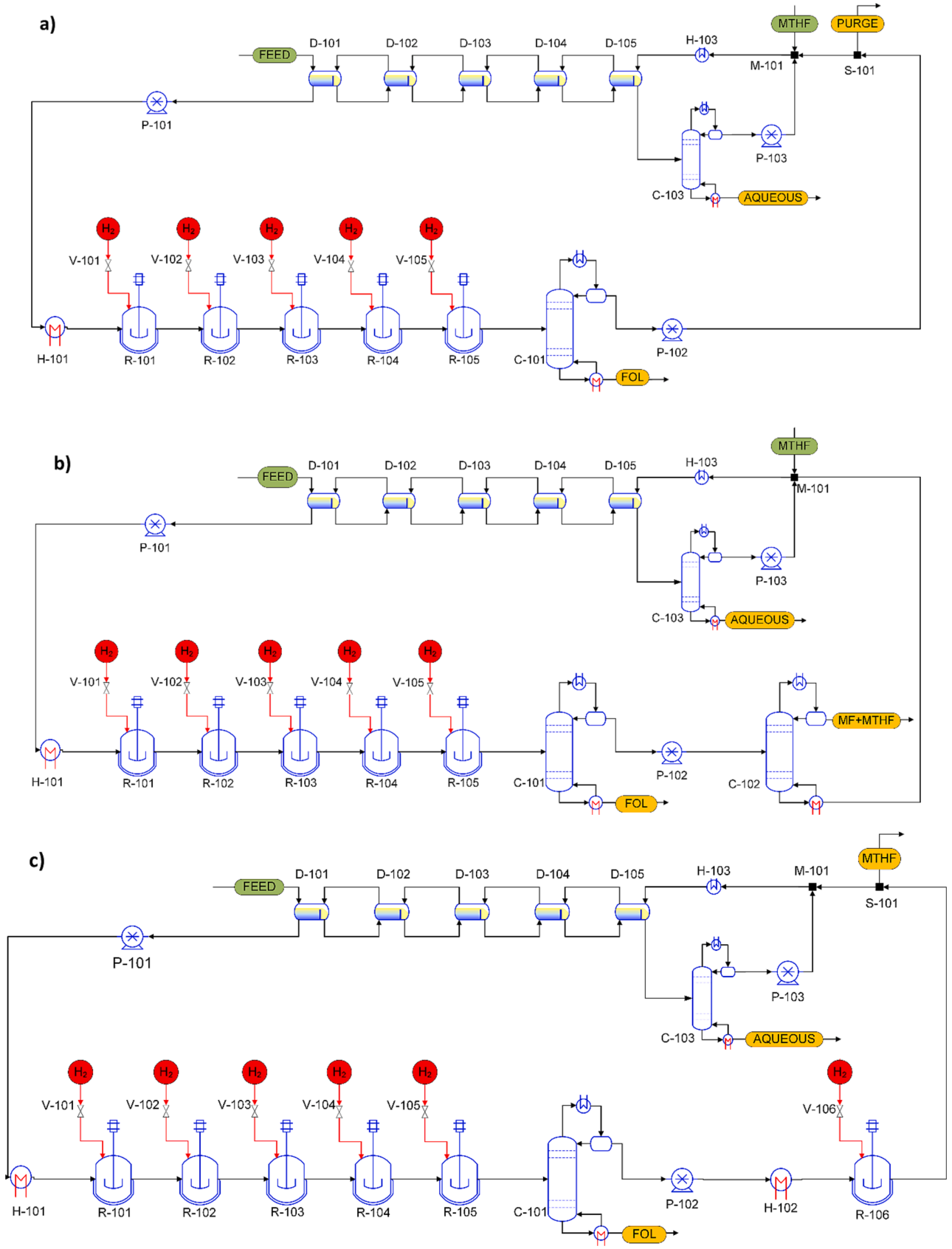

Fig. 4. Flowsheet diagram of a) CASE I: purging of the C-101 distillate stream, b) CASE II: separating MF from MTHF by means of distillation in C-102, and c) CASE III: incorporating the conversion of MF into MTHF in R-106.

Table 6
Energy requirements for MF separation (CASE II) or MF conversion (CASE III).

	Heating energy (kJ/s)	Cooling energy(kJ/s)
Case II	1369	−1047.4
Case III	688	−257

benefits from an environmental perspective due to the use of a commercial non-toxic catalyst and the net production of a green solvent, MTHF.

The literature on alternative production methods for FOL is somewhat limited. Byun et al. [59] propose a combined approach that synthesizes FOL and glycerol oxygenates simultaneously with hydrogen in an electrocatalytic oxidation process. While their method resembles the current FOL production process, the innovation lies in its integration with the glycerol electrocatalytic oxidation process. Despite its straightforward FOL production, their process generates a residual waste stream accounting for 4 % of the organic matter, comprised of 40 wt% FUR, 40 wt% MF, and 20 wt% FOL.

Conversely, the method described in this study operates at lower temperatures, eliminating the generation of these waste streams and reducing FUR loss. Additionally, this process efficiently converts the MF produced into MTHF, avoiding its accumulation and achieving a net production of a green solvent.

It is crucial for techno-economic assessments to ascertain the impact of multiple parameters on the final MSP to determine the most critical factors for establishing a viable process. To this end, sensitivity analyses were conducted, involving ± 30 % variations in the prices of FUR and hydrogen, along with assessments of capital and utility costs. Global geopolitical instability in recent years has led to substantial fluctuations in energy prices, prompting an investigation into their effect on the final MSP. Additionally, given the inherent uncertainties in estimating CapEx at this level [38], their influence was carefully examined.

Fig. 7 shows that changes in FUR prices predominantly drive variations in the MSP. This is consistent with the fact that raw materials costs account for nearly 65 % of total expenditure. It is essential to note that fluctuations in FUR prices affect every FOL production plant uniformly, without necessarily favoring one alternative over another. Moreover, the study has found that variations in CapEx, utility expenses, and H_2 prices do not significantly alter MSP values. This aspect bodes well, indicating that the process's dependence on these parameters is minimal.

4. Conclusions

The process developed here for the liquid phase production of FOL includes an initial liquid–liquid extraction unit. MTHF effectively extracts FUR from an aqueous phase with the same concentration as the one obtained after a conventional steam-stripping hydrolysis reaction. After fine-tuning the countercurrent mixer-settler extraction unit, the concentration of FUR in the extract increases to 15 wt% with a water content of around 5 wt%. The solvent present in the raffinate is easily recovered by distillation. Regarding the reaction section, activity test results using commercial CuZnAl catalyst recorded very high selectivity

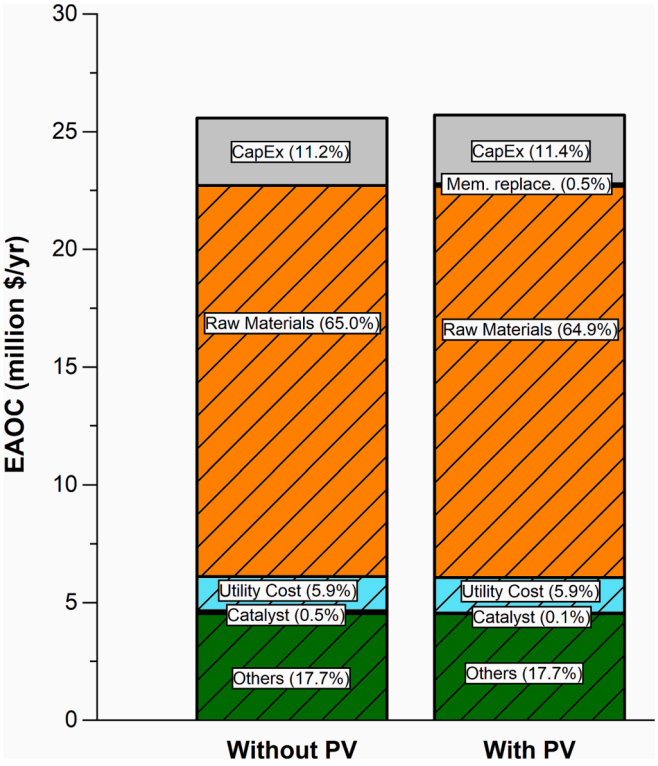

Fig. 6. Distribution of EAOC between CapEx (plain) and OpEx (pattern blocks).

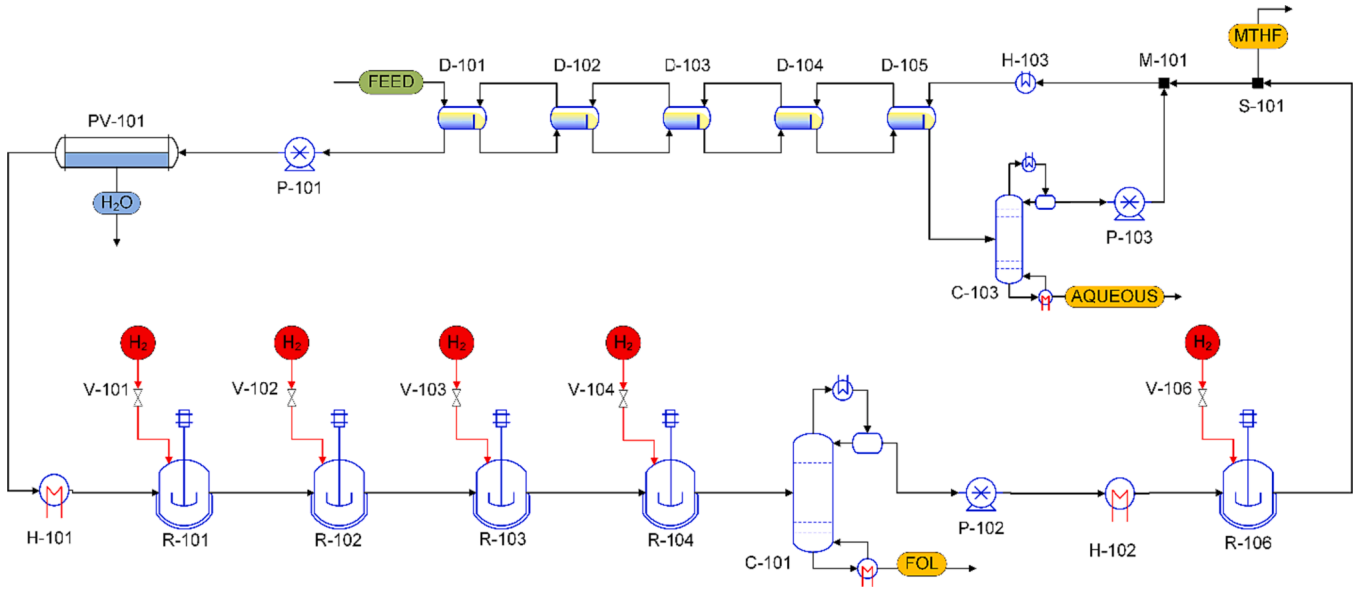

Fig. 5. Flowsheet diagram of CASE III (conversion of MF into MTHF), incorporating the PV module.

Table 7
Cost analysis of the FOL production process from FUR considering the installation with or without a PV membrane module.

	CapEx ($)			
	Without PV		**With PV**	
LL extraction	2,616,300	44 %	2,615,500	42 %
PV membrane module	–	–	1,210,782	19 %
Reaction section	2,269,600	38 %	1,389,200	22 %
FOL purification	773,200	13 %	698,100	11 %
MF treatment	347,400	6 %	335,500	5 %
Total Installed Cost	6,006,500		6,249,082	
Added costs [a]	5,985,300		5,985,300	
Total CapEx	11,991,800		12,234,382	
Annualized CapEx ($/year)	2,860,317		2,918,179	
[a] Indirect costs, plus contingency and fee costs, and auxiliary facilities.				
	OpEx ($/year)			
	Without PV		**With PV**	
Raw Materials	16,609,945	73.3 %	16,609,945	73.3 %
Utilities Cost	1,455,540	6.4 %	1,388,618	6.1 %
Catalyst	63.346	0.6 %	19.161	<0.1 %
Membrane replacement	–	–	119,104	0.5 %
Others [b]	4,520,360	20.0 %	4,520,360	20.0 %
OpEx	22,649,191		22,657,189	
[b] Operating labor, maintenance, overheads…				
	Final economic assessment			
	Without PV		**With PV**	
EAOC ($/year)	25,572,853		25,575,368	
FOL production capacity (t/year)	19,750		19,750	
MSP ($/t)	1,347 (1,349[c])		1,348 (1,326[d])	
[c] Considering the aqueous MTHF treatment				
[d] Considering the sale of MTHF as income				

to the target product, and MF was the only by-product detected, and in very low yields. The kinetic study developed and validated a double-site Langmuir-Hinshelwood, including the effect of low water content. Water reduces the reaction rate by competing for active sites with FUR and FOL. Interestingly, the low water concentration assayed does not promote the formation of any by-products other than MF. The fine-tuning of the reactors allowed the production of FOL in a high 97 % yield. In the final purification section, the best option for recirculating the solvent was to transform MF into MTHF to avoid the accumulation of the former and obtain a net production of the green solvent. The preliminary economic analysis revealed a promising FOL MSP of 1,326 $/t, which is only 30 % higher than the FUR price considered in the calculations. In addition, the process addresses the main environmental issues surrounding industrial FOL production: it minimizes energy use in the intermediate and final purification stages, reduces toxic solid waste by using a chromite-free catalyst, and co-produces a green solvent. In this way, it contributes to advancing the sustainability of processes using furfural as a platform molecule.

Declaration of competing interest

The authors declare that they have no known competing financial interests or personal relationships that could have appeared to influence the work reported in this paper.

Data availability

Data will be made available on request.

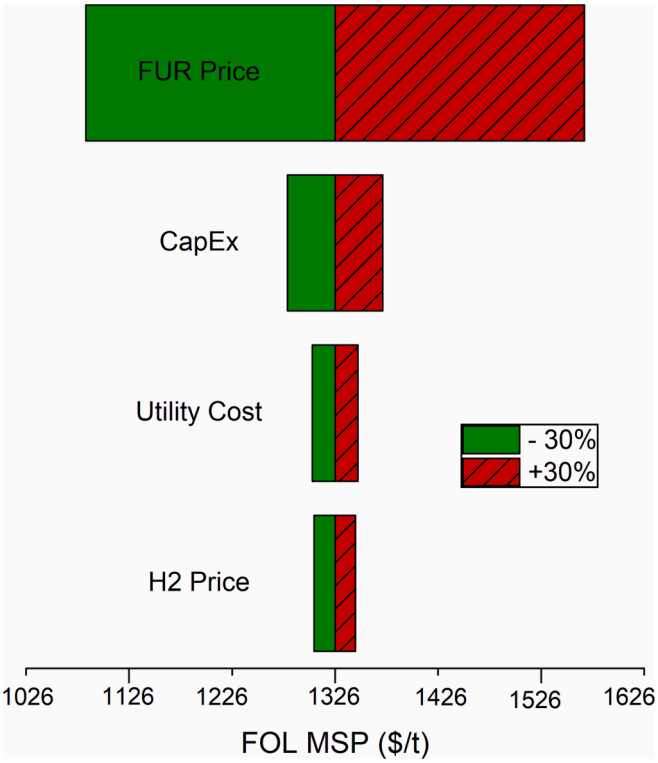

Fig. 7. Sensitivity analysis on the FOL MSP.

Acknowledgements

This work was supported by the University of the Basque Country (UPV/EHU), the European Union, through the European Regional Development Fund, the Spanish National Research Agency - Agencia Estatal de Investigación: PID-2021-122736OB-C43), and the Basque Government (Project IT1554-22).

Appendix A. Supplementary data

Supplementary data to this article can be found online at https://doi.org/10.1016/j.cej.2023.147873.

References

[1] Y. Panchaksharam, J. Spekreijse, R. Chinthapalli, C Vom Berg, Business cases: Case studies on potentially attractive opportunities for bio-based chemicals in Europe, (2018). https://doi.org/10.13140/RG.2.2.16896.92168.
[2] A. Jaswal, P.P. Singh, T. Mondal, Furfural-a versatile, biomass-derived platform chemical for the production of renewable chemicals, Green Chem. 24 (2022) 510–551, https://doi.org/10.1039/d1gc03278j.
[3] C. S. Miner, H. J. Brownlee, Process of manufacturing furfural (U.S. Patent No. 17.350.84A), 1922.
[4] K.J. Zeitsch, The Chemistry and Technology of Furfural and its Many By-Products, Elsevier, 2000.
[5] J.-S. Hwang, A. Singh Mamman, J.-M. Lee, Y.-C. Kim, I. Taek Hwang, N.-J. Park, Y. Kyu Hwang, J.-S. Chang, Furfural: Hemicellulose/xylose-derived biochemical, Bioprod Bioref. 2 (2008) 438–454, https://doi.org/10.1002/bbb.95.
[6] R. Mariscal, P. Maireles-Torres, M. Ojeda, I. Sádaba, M. López Granados, Furfural: A renewable and versatile platform molecule for the synthesis of chemicals and fuels, Energy Environ Sci. 9 (2016) 1144–1189, https://doi.org/10.1039/c5ee02666k.
[7] J.P. Lange, E. Van Der Heide, J. Van Buijtenen, R. Price, Furfural-A promising platform for lignocellulosic biofuels, ChemSusChem 5 (2012) 150–166, https://doi.org/10.1002/cssc.201100648.
[8] A.P. Dunlop, F.N. Peters Jr., The Nature of Furfuryl Alcohol, Ind. Eng. Chem. 34 (1942) 814–817, https://doi.org/10.1021/ie50391a010.
[9] J.B. Barr, S.B. Wallon, The chemistry of furfuryl alcohol resins, J. Appl. Polym. Sci. 15 (1971) 1079–1090, https://doi.org/10.1002/app.1971.070150504.
[10] H.E. Hoydonckx, W.M. Van Rhijn, D.E.E. De Vos, P.A. Jacobs, Furfural and derivatives, in: Ullmann's Encyclopedia of Industrial Chemistry, Wiley-VCH Verlag GmbH & Co KGaA, 2007, pp. 335–340, 10.1002/14356007.a12_119.pub2.

[11] M. Kalong, S. Ratchahat, P. Khemthong, S. Assabumrungrat, A. Srifa, Effect of co-doping on Cu/CaO catalysts for selective furfural hydrogenation into furfuryl, Alcohol (2022), https://doi.org/10.3390/nano12091578.

[12] X. Gao, Y. Ding, L. Peng, D. Yang, X. Wan, C. Zhou, W. Liu, Y. Dai, Y. Yang, On the effect of zeolite acid property and reaction pathway in Pd–catalyzed hydrogenation of furfural to cyclopentanone, Fuel 314 (2022), https://doi.org/10.1016/j.fuel.2021.123074.

[13] M. Hronec, K. Fulajtárová, I. Vávra, T. Soták, E. Dobročka, M. Mičušík, Carbon supported Pd-Cu catalysts for highly selective rearrangement of furfural to cyclopentanone, Appl. Catal. B. 181 (2016) 210–219, https://doi.org/10.1016/j.apcatb.2015.07.046.

[14] S. Thongratkaew, S. Kiatphuengporn, A. Junkaew, S. Kuboon, N. Chanlek, A. Seubsai, B. Rungtaweevoranit, K. Faungnawakij, Solvent effects in integrated reaction-separation process of liquid-phase hydrogenation of furfural to furfuryl alcohol over $CuAl_2O_4$ catalysts, Catal. Commun. 169 (2022), 106468, https://doi.org/10.1016/j.catcom.2022.106468.

[15] S. Xia, Y. Li, Q. Shang, C. Zhang, P. Ma, Liquid-phase catalytic hydrogenation of furfural in variable solvent media, Trans. Tianjin Univ. 22 (2016) 202–210, https://doi.org/10.1007/s12209-016-2804-x.

[16] M.M. Villaverde, T.F. Garetto, A.J. Marchi, Liquid-phase transfer hydrogenation of furfural to furfuryl alcohol on Cu–Mg–Al catalysts, Catal. Commun. 58 (2015) 6–10, https://doi.org/10.1016/J.CATCOM.2014.08.021.

[17] I. Gandarias, S. García-Fernández, I. Obregón, I. Agirrezabal-Telleria, P.L. Arias, Production of 2-methylfuran from biomass through an integrated biorefinery approach, Fuel Process. Technol. 178 (2018) 336–343, https://doi.org/10.1016/j.fuproc.2018.05.037.

[18] A. Barranca, I. Agirrezabal-Telleria, M. Rellán-Piñeiro, M.A. Ortuño, I. Gandarias, Selective furfural hydrogenolysis towards 2-methylfuran by controlled poisoning of Cu-Co catalysts with chlorine, React. Chem. Eng. 8 (2022) 687–698, https://doi.org/10.1039/d2re00414c.

[19] I. Obregón, I. Gandarias, N. M. Miletić, A. Ocio, P. L. Arias, One-Pot 2-Methyltetrahydrofuran Production from Levulinic Acid in Green Solvents Using Ni-Cu/Al_2O_3 *Catalysts*, (n.d.). https://doi.org/10.1002/cssc.201500671.

[20] V. Pace, P. Hoyos, L. Castoldi, P. Domínguez de María, A. R. Alcántara, 2-Methyltetrahydrofuran (2-MeTHF): A Biomass-Derived Solvent with Broad Application in Organic Chemistry, (n.d.). https://doi.org/10.1002/cssc.201100780.

[21] E.K. New, S.K. Tnah, K.S. Voon, K.J. Yong, A. Procentese, K.P. Yee Shak, W. Subramonian, C.K. Cheng, T.Y. Wu, The application of green solvent in a biorefinery using lignocellulosic biomass as a feedstock, J. Environ. Manage. 307 (2022), 114385, https://doi.org/10.1016/j.jenvman.2021.114385.

[22] S. Sitthisa, T. Sooknoi, Y. Ma, P.B. Balbuena, D.E. Resasco, Kinetics and mechanism of hydrogenation of furfural on Cu/SiO2 catalysts, J. Catal. 277 (2011) 1–13, https://doi.org/10.1016/j.jcat.2010.10.005.

[23] C.P. Jiménez-Gómez, J.A. Cecilia, A.C. Alba-Rubio, A. Cassidy, R. Moreno-Tost, C. García-Sancho, P. Maireles-Torres, Tailoring the selectivity of Cu-based catalysts in the furfural hydrogenation reaction: Influence of the morphology of the silica support, Fuel 319 (2022), 123827, https://doi.org/10.1016/J.FUEL.2022.123827.

[24] G. Singh, L. Singh, J. Gahtori, R.K. Gupta, C. Samanta, R. Bal, A. Bordoloi, Catalytic hydrogenation of furfural to furfuryl alcohol over chromium-free catalyst: Enhanced selectivity in the presence of solvent, Mol. Catal. 500 (2021), 111339, https://doi.org/10.1016/j.mcat.2020.111339.

[25] M.J. Islam, M. Granollers Mesa, A. Osatiashtiani, M.J. Taylor, J.C. Manayil, C.M. A. Parlett, M.A. Isaacs, G. Kyriakou, The effect of metal precursor on copper phase dispersion and nanoparticle formation for the catalytic transformations of furfural, Appl Catal B 273 (2020), 119062, https://doi.org/10.1016/j.apcatb.2020.119062.

[26] J. Zhang, Z. Jia, S. Yu, S. Liu, L. Li, C. Xie, Q. Wu, Y. Zhang, H. Yu, Y. Liu, J. Pang, Y. Liu, Regulating the Cu0-Cu+ ratio to enhance metal-support interaction for selective hydrogenation of furfural under mild conditions, Chem. Eng. J. 468 (2023), https://doi.org/10.1016/j.cej.2023.143755.

[27] S. Liu, N. Govindarajan, K. Chan, Understanding Activity Trends in Furfural Hydrogenation on Transition Metal Surfaces, ACS Catal. 12 (2022) 12902–12910, https://doi.org/10.1021/acscatal.2c03822.

[28] C.P. Jiménez-Gómez, J.A. Cecilia, C. García-Sancho, R. Moreno-Tost, P. Maireles-Torres, Gas phase hydrogenation of furfural to obtain valuable products using commercial Cr-free catalysts as an environmentally sustainable alternative to copper chromite, J. Environ. Chem. Eng. 9 (2021), 105468, https://doi.org/10.1016/J.JECE.2021.105468.

[29] J. Slak, B. Pomeroy, A. Kostyniuk, M. Grilc, B. Likozar, A review of bio-refining process intensification in catalytic conversion reactions, separations and purifications of hydroxymethylfurfural (HMF) and furfural, Chem. Eng. J. 429 (2022), https://doi.org/10.1016/j.cej.2021.132325.

[30] M. Männistö, J.P. Pokki, L. Fournis, V. Alopaeus, Ternary and binary LLE measurements for solvent (2-methyltetrahydrofuran and cyclopentyl methyl ether) + furfural + water between 298 and 343 K, J. Chem. Thermodyn. 110 (2017) 127–136, https://doi.org/10.1016/j.jct.2017.02.016.

[31] J.G. Hayden, J.P. O'Connell, A Generalized Method for Predicting Second Virial Coefficients, Ind. Eng. Chem. Process Des. Dev. 14 (1975) 209–216, https://doi.org/10.1021/i260055a003.

[32] F. Aage, R.L. Jones, J.M. Prausnitz, Group-contribution estimation of activity coefficients in nonideal liquid mixtures, AIChE J 21 (1975) 1086–1099, https://doi.org/10.1002/aic.690210607.

[33] W.L. Luyben, Distillation design and control using aspen simulations, 2nd Edition, John Wiley & Sons, Hoboken, New Jersey, 2013.

[34] I. Agirre, M. B. Güemez, H. M. Van Veen, A. Motelica, J. F. Vente, P. L. Arias, A techno-economic comparison of the various processes for the production of 1,1 diethoxy butane, in: *XIX International Symposium on Alcohol Fuels* (ISAF XIX); 10 - 14 October, 2011; Verona (Italy), 2011.

[35] I. Agirre, M.B. Güemez, H.M. Van Veen, A. Motelica, J.F. Vente, P.L. Arias, Conceptual Design of a Membrane Reactor for Continuous Production of 1,1 Diethoxy Butane, a Bio-Based Oxygenated Diesel. International Congress on Membranes and Membrane Processes. ICOM 2011; 23-29 July, 2011; Amsterdam, 2011.

[36] I. Agirre, M.B. Güemez, H.M. van Veen, A. Motelica, J.F. Vente, P.L. Arias, Acetalization reaction of ethanol with butyraldehyde coupled with pervaporation. Semi-batch pervaporation studies and resistance of HybSi® membranes to catalyst impacts, J Memb Sci. 371 (2011) 179–188.

[37] F.K. Kazi, A.D. Patel, J.C. Serrano-Ruiz, J.A. Dumesic, R.P. Anex, Techno-economic analysis of dimethylfuran (DMF) and hydroxymethylfurfural (HMF) production from pure fructose in catalytic processes, Chem. Eng. J. 169 (2011) 329–338, https://doi.org/10.1016/j.cej.2011.03.018.

[38] R. Turton, R.C. Bailie, W.B. Whiting, J.A. Shaeiwitz, D. Bhattacharyya, Analysis, Synthesis, and Design of Chemical Processes, 4th ed., Prentice Hall, Upper Saddle River, New Jersey, 2012.

[39] V. Van Hoof, L. Van den Abeele, A. Buekenhoudt, C. Dotremont, R. Leysen, Economic comparison between azeotropic distillation and different hybrid systems combining distillation with pervaporation for the dehydration of isopropanol, Sep. Purif. Technol. 37 (2004) 33–49, https://doi.org/10.1016/j.seppur.2003.08.003.

[40] Dutch Association of Cost Engineers (DACE) Price Booklet: A publication of Reed Business, 27th Ed., The Hague, 2009.

[41] M.S. Peters, K.D. Timmerhaus, R.E. West, Plant Design and Economics for Chemical Engineers, 5th Ed., McGraw-Hill, New York, 2003.

[42] D.M. Alonso, S.H. Hakim, S. Zhou, W. Won, O. Hosseinaei, J. Tao, V. Garcia-Negron, A.H. Motagamwala, M.A. Mellmer, K. Huang, C.J. Houtman, N. Labbé, D. P. Harper, C. Maravelias, T. Runge, J.A. Dumesic, Increasing the revenue from lignocellulosic biomass : Maximizing feedstock utilization, Sci. Adv. 3 (2017), https://doi.org/10.1126/sciadv.1603301.

[43] M.Z.R. Mohammed, Z.W. Ng, A. Putranto, Z.Y. Kong, J. Sunarso, M. Aziz, S.H. Zein, J. Giwangkara, I. Butar, Process design, simulation, and techno-economic analysis of integrated production of furfural and glucose derived from palm oil empty fruit bunches, *Clean Technol Environ*, Policy 25 (2023) 1551–1567, https://doi.org/10.1007/s10098-022-02454-3.

[44] I. Agirre, I. Gandarias, M.L. Granados, P.L. Arias, Process design and techno-economic analysis of gas and aqueous phase maleic anhydride production from biomass-derived furfural, Biomass Convers. Biorefin. 10 (2020), https://doi.org/10.1007/s13399-019-00462-w.

[45] R.P. Bangalore Ashok, P. Oinas, S. Forssell, Techno-economic evaluation of a biorefinery to produce γ-valerolactone (GVL), 2-methyltetrahydrofuran (2-MTHF) and 5-hydroxymethylfurfural (5-HMF) from spruce, Renew, Energy 190 (2022) 396–407, https://doi.org/10.1016/j.renene.2022.03.128.

[46] J.F. Leal Silva, A.P. Mariano, R., Maciel Filho, Economic potential of 2-methyltetrahydrofuran (MTHF) and ethyl levulinate (EL) produced from hemicelluloses-derived furfural, Biomass Bioenergy 119 (2018) 492–502, https://doi.org/10.1016/j.biombioe.2018.10.008.

[47] A. Al Ghatta, J.D.E.T. Wilton-Ely, J.P. Hallett, From sugars to FDCA: a techno-economic assessment using a design concept based on solvent selection and carbon dioxide emissions, Green Chem. 23 (2021) 1716–1733, https://doi.org/10.1039/d0gc03991h.

[48] M.M. Villaverde, N.M. Bertero, T.F. Garetto, A.J. Marchi, Selective liquid-phase hydrogenation of furfural to furfuryl alcohol over Cu-based catalysts, Catal. Today (2013) 87–92, https://doi.org/10.1016/j.cattod.2013.02.031.

[49] R.V. Sharma, U. Das, R. Sammynaiken, A.K. Dalai, Liquid phase chemo-selective catalytic hydrogenation of furfural to furfuryl alcohol, Appl. Catal. A 454 (2013) 127–136, https://doi.org/10.1016/j.apcata.2012.12.010.

[50] S. Srivastava, N. Solanki, P. Mohanty, K.A. Shah, J.K. Parikh, A.K. Dalai, Optimization and Kinetic Studies on Hydrogenation of Furfural to Furfuryl Alcohol over SBA-15 Supported Bimetallic Copper-Cobalt Catalyst, Catal Letters. 145 (2015) 816–823, https://doi.org/10.1007/s10562-015-1488-5.

[51] R. Šivec, M. Huš, B. Likozar, M. Grilc, Furfural hydrogenation over Cu, Ni, Pd, Pt, Re, Rh and Ru catalysts: Ab initio modelling of adsorption, desorption and reaction micro-kinetics, Chem. Eng. J. 436 (2022), 135070, https://doi.org/10.1016/j.cej.2022.135070.

[52] S. Srivastava, G.C. Jadeja, J.K. Parikh, Copper-cobalt catalyzed liquid phase hydrogenation of furfural to 2-methylfuran: An optimization, kinetics and reaction mechanism study, Chem. Eng. Res. Des. 16 (2018) 313–324, https://doi.org/10.1016/j.cherd.2018.01.031.

[53] P. Liu, W. Qiu, C. Zhang, Q. Tan, C. Zhang, W. Zhang, Y. Song, H. Wang, C. Li, Kinetics of Furfural Hydrogenation over Bimetallic Overlayer Catalysts and the Effect of Oxygen Vacancy Concentration on Product Selectivity, ChemCatChem 11 (2019) 3296–3306, https://doi.org/10.1002/cctc.201900625.

[54] M. Pirmoradi, J.R. Kastner, A kinetic model of multi-step furfural hydrogenation over a Pd-TiO2 supported activated carbon catalyst, Chem. Eng. J. 414 (2021), 128693, https://doi.org/10.1016/j.cej.2021.128693.

[55] P.D. Vaidya, V.V. Mahajani, Kinetics of liquid-phase hydrogenation of furfuraldehyde to furfuryl alcohol over a Pt/C catalyst, Ind. Eng. Chem. Res. 42 (2003) 3881–3885, https://doi.org/10.1021/ie030055k.

[56] R.S. Rao, R. Terry, K. Baker, M. Albert Vannice, Furfural hydrogenation over carbon-supported copper, Catal Letters. 60 (1999) 51–57.

[57] M. Ghashghaee, S. Shirvani, M. Ghambarian, Kinetic models for hydroconversion of furfural over the ecofriendly Cu-MgO catalyst: An experimental and theoretical

study, Appl. Catal. A 545 (2017) 134–147, https://doi.org/10.1016/j.apcata.2017.07.040.
[58] J.P. Lange, Catalysis for biorefineries-performance criteria for industrial operation, *Catal*, Sci. Technol. 6 (2016) 4759–4767, https://doi.org/10.1039/c6cy00431h.
[59] J. Byun, D. Kim, D. Lee, H.J. Kim, J. Han, Integrated strategy for concurrent production of furfuryl alcohol and glycerol oxygenates, J. Ind. Eng. Chem. 73 (2019) 268–275, https://doi.org/10.1016/j.jiec.2019.01.038.